Biophysical Chemistry 16 (1982) 41–49
Elsevier Biomedical Press

THEORY OF SEDIMENTATION FOR LIGAND-MEDIATED HETEROGENEOUS ASSOCIATION-DISSOCIATION REACTIONS

John R. CANN

Department of Biochemistry/Biophysics/Genetics, University of Colorado Health Sciences Center, 4200 E. 9th Avenue, Denver, CO 80262, U.S.A.

Received 22nd March 1982
Accepted 23rd April 1982

Key words: Sedimentation theory; Ligand mediation; Heterogeneous association; Self-association; Protein assembly; Subunit protein

Theoretical analytical sedimentation patterns have been computed for ligand-mediated heterogeneous association-dissociation reactions between macromolecules. Involvement of either a single kind of ligand or two different ligands acting in a stepwise fashion has been considered. Self-association, mediated in a stepwise fashion by two different ligands, has also been examined. The conclusion reached is that such interactions have the potentiality for exhibiting as many as three or four sedimenting peaks despite rapid rates of reaction. In general, the peaks correspond to different equilibrium compositions and not to individual macromolecular species; that is to say, they constitute a reaction boundary. Their resolution depends upon generation of concentration gradients of ligand(s) along the centrifuge cell by chemical reequilibration during sedimentation of the several macromolecular species. The implications of these findings for fundamental studies on subunit proteins and protein assemblies and for conventional applications of ultracentrifugation are discussed.

1. Introduction

Previously [1–4], we elaborated a phenomenological theory of sedimentation for reversible ligand-mediated self-association of the type

$$mM + nX \rightleftharpoons M_mX_n \quad (1)$$

in which a macromolecule, M, associates into an m-mer, with the mediation of a small ligand molecule, X, of which a fixed number, n, are bound into the complex. Of particular interest is ligand-mediated dimerization; i.e., $m = 2$. Thus, in contradistinction to simple dimerization

$$2M \rightleftharpoons M_2 \quad (2)$$

which always gives sedimentation patterns showing a single peak when chemical equilibration is rapid [5–10], ligand-mediated dimerization can give a well resolved bimodal reaction boundary or zone even for fast rates of reaction. Resolution of the two peaks depends upon the production and maintenance of concentration gradients of unbound ligand along the centrifuge cell by reequilibration during differential sedimentation of macromonomer and dimer; and the peaks correspond to different equilibrium mixtures of monomer and dimer. These theoretical predictions have been confirmed experimentally in the case of the interaction of vinblastine with tubulin [11]. Of course, for sufficiently weak interactions (i.e., sufficiently high ligand concentrations) or low centrifugal field, ligand-mediated dimerization can also give patterns that show a single peak. In the limit where, for any reason, the concentration of unbound ligand along the centrifuge cell is not signifcantly perturbed by reaction during differential sedimentation of macromonomer and dimer, the sedimentation behavior approaches that of the simple dimerization reaction 2.

These several results suggest that the possible involvement of ligands in certain heterogeneous association-dissociation reactions might also play

a dominant role in determining the sedimentation behavior of such systems. Examples of complex formation between different proteins influenced in one way or another by small ligand molecules or ions include: the structural role of Zn^{2+} in stabilizing the quaternary structure of nerve growth factor, which is composed of nonidentical protein subunits [12]; the structural role of Mg^{2+} in stabilizing the subunit structure of the *Escherichia coli* regulatory enzyme, ribonucleotide-diphosphate reductase [13]; the role of metals in determining the quaternary structure of the regulatory enzyme glutamine synthetase from *E. coli* [14]; the Ca^{2+} sensitivity of the troponin complex [15,16]; modification of the interaction of myosin subfragments with actin by Ca^{2+} [17] and by nucleotides [18]; and the Ca^{2+}-dependent binding of calmodulin to the phosphodiesterase or troponin I [19,20]. Each of these interactions evidently involves a single kind of ligand, but it is conceivable that the stability of some protein assemblies might depend upon two different ligands. Accordingly, a theoretical investigation has been made of the analytical sedimentation behavior of model heterogeneous associations mediated by either a single kind of ligand or two different ligands acting in a stepwise fashion. In addition, self-association mediated in a stepwise fashion by two different ligands has been examined. All reactions are assumed to be reversible, and the calculations are for the limit of instantaneous reestablishment of equilibrium during differential transport of the macromolecular species. The results of these calculations are reported below.

2. Theory

Two model heterogeneous associating-dissociating systems have been considered. In the first model, association is mediated in part by a single kind of ligand as schematized by the reaction set

$$A+B \rightleftharpoons AB, \quad K_1 \tag{3a}$$

$$AB+D+X \rightleftharpoons ABDX, \quad K_2 \tag{3b}$$

where A, B and D are three different protein molecules. The special cases in which D is identical with either A or B have also been examined. The second model is for mediation by two different ligands,

$$A+B+X \rightleftharpoons ABX, \quad K_1 \tag{4a}$$

$$2ABX+Y \rightleftharpoons (ABX)_2Y, \quad K_2 \tag{4b}$$

in which ligand X is obligatory for complex formation between proteins A and B, and ligand Y is obligatory for dimerization of the complex ABX. Note that in the absence of Y reaction set 4 collapses to the simple ligand-mediated heterogeneous association reaction 4a. The model for self-association mediated by two different ligands is for the tetramerization schema,

$$2M+X \rightleftharpoons M_2X, \quad K_1 \tag{5a}$$

$$2M_2X+Y \rightleftharpoons (M_2X)_2Y, \quad K_2 \tag{5b}$$

In the absence of Y this reaction set collapses to the ligand-mediated dimerization reaction 5a; i.e., to the previously considered reaction 1 with $m=2$ and $n=1$. The calculations for each of these three reaction sets were accompanied by control calculations on an analogous association schema but without mediation by ligand(s), the control association schema for reaction set 3 being

$$A+B \rightleftharpoons AB, \quad K_1 \tag{6a}$$

$$AB+D \rightleftharpoons ABD, \quad K_2 \tag{6b}$$

and so on.

Theoretical analytical sedimentation patterns have been computed by numerical solution of the appropriate set of simultaneous transport equations and mass action expressions. In the case of reaction set 3 in a sector-shaped centrifuge cell, for example, the set of equations is

$$\frac{\partial C_i}{\partial t} = \frac{1}{r}\frac{\partial}{\partial r}\left[\left(D_i\frac{\partial C_i}{\partial r} - C_i s_i \omega^2 r\right) r\right] \tag{7a}$$

$$\frac{\partial C_6}{\partial t} = \frac{1}{r}\frac{\partial}{\partial r}\left[\left(D_6\frac{\partial C_6}{\partial r}\right) r\right] \tag{7b}$$

$$K_1 = C_3/C_1C_2 \tag{7c}$$

$$K_2 = C_6/C_3C_4C_5 \tag{7d}$$

in which C designates molar concentration; D, diffusion coefficient; s, sedimentation coefficient; ω, angular velocity; r, radial distance; and t, time. The subscripts $i=1,2\ldots5$ designate the macromolecular species A, B, AB, D and ABDX, respectively; and the subscript 6 designates unbound

ligand, X, whose sedimentation coefficient is taken to be zero. Eqs. 7a and 7b conserve macromolecule and ligand by taking into account diffusion and transport in the centrifugal field. Eqs. 7c and 7d express the effect of reactions 3a and 3b on the concentrations. Eqs. 7 were solved for C_i and C_6 as functions of r and t; and the theoretical sedimentation patterns are displayed as plots of $\partial c/\partial r$ vs. r, where $c = 10^{-3} \cdot \Sigma^i M_i C_i$ is the total macromolecule concentration in g/ml, and M is the molecular weight. The positions of the meniscus, r_m, and the bottom of the centrifuge cell, r_b, are indicated in the abscissa. Vertical arrows at the top of the figures indicate where the peaks in the patterns would have been located had sedimentation been carried out on a mixture of noninteracting macromolecules having the same sedimentation coefficients as the interacting species. The molar concentration of unbound ligand, $[X] \equiv C_6$, along the centrifuge cell is also shown.

For calculations to the rectilinear and constant field approximations in a moving coordinate system, the transport eqs. 7a and 7b take the form

$$\frac{\partial C_i}{\partial t} = D_i \frac{\partial^2 C_i}{\partial x'^2} - (v_i - v_c)\frac{\partial C_i}{\partial x'} \tag{8a}$$

$$\frac{\partial C_6}{\partial t} = D_6 \frac{\partial^2 C_6}{\partial x'^2} + v_c \frac{\partial C_6}{\partial x'} \tag{8b}$$

in which $v_i = s_i \omega^2 \bar{x}$, where $\bar{x} = 6.5$ cm; v_c is the velocity of the coordinate system chosen so as to center the sedimentation pattern in the coordinate system, its value being approximately the average of v_i of all macromolecular species; and $x' = x - v_c t$ is the position in the moving coordinate system, where x is the position in the static system. Here, the sedimentation patterns are displayed as plots of $\partial c/\partial x$ vs. x'.

Since the numerical procedures used to solve eqs. 7 and 8 are described in detail elsewhere for several illustrative, rapidly equilibrating systems [4,10,21,22], only a few qualitative comments are warranted here. The calculations for sedimentation in a sector-shaped ultracentrifuge cell follow the numerical formulation of Goad [21] in using (1) a moving coordinate system with uniformly logarithmic spacing and (2) higher-order differencing of the transport equations with the Archibald condition applied at the meniscus and the bottom of the cell. The diffusion current was calculated explicitly rather than implicitly, so that in order to ensure stability $\Delta r \simeq 0.006$ cm and $\Delta t \simeq 1$s were assigned much smaller values than used by Goad. Test calculations showed that the uncoupled species sedimented and diffused accurately and that radial dilution was accurate to about 0.006%. Material balance was excellent.

Calculations to the rectilinear and constant field approximations in a moving coordinate system employ the method of first differences [4], corrections being made for the major fraction of the truncation error due to the way the first spatial derivative in the transport equations is approximated [21,22]. The error here is not much different than for a sector-shaped cell. In both cases the driven and diffusion currents are accurate to Δr^3 and Δr^2, respectively; and the overall error due to time differencing is of the order Δt. There were no qualitative differences between patterns calculated to the rectilinear-constant field approximation and those for a sector-shaped cell, which differ significantly only in the relative areas of the peaks due to radial dilution in the latter. (Compare pattern b in fig. 4B with pattern a in fig. 4A.)

The hydrodynamic dependence of sedimentation and diffusion coefficients upon macromolecule concentration was ignored, because we did not wish to introduce additional adjustable parameters into the calculation. This is justified by our previous finding [3] that inclusion of the concentration dependence of the transport coefficients does not prevent resolution of the bimodal reaction boundary calculated for ligand-mediated dimerization.

Computations were made on the University of Colorado's Cyber 172 electronic computer. Transport and molecular parameters are given in the figure legends along with constituent concentration of reactants, designated as $\bar{A}$, $\bar{X}$, etc.

Finally, as a prelude to the presentation of the results of the calculations, a few words regarding the shape of the analytical sedimentation patterns expected for reacting systems are in order. Consider, for example, the heterogeneous association-dissociation reaction $A + B \rightleftharpoons AB$, where the sedimentation coefficients, $s_A < s_B < s_{AB}$, and reactant

A is in molar excess. The shape of the pattern will depend upon the rate of reequilibration during differential sedimentation of A, B and AB. There are two limiting cases. The first case is for rates of reaction so slow that negligible association-dissociation occurs during the course of the sedimentation experiment. In this limit, the system behaves like a mixture of three noninteracting proteins. Thus, the pattern shows three peaks (i.e., sedimenting boundaries): a slowly sedimenting peak of pure A, a more rapidly sedimenting peak corresponding to uncombined B, and a still faster peak of AB. The other limit, which is of interest here, is for rates of reaction sufficiently fast that the reaction is at equilibrium at every position along the centrifuge cell at every instant of time. In this case, the pattern will exhibit only two peaks [23]: a boundary of pure A and a peak sedimenting at a logarithmic velocity intermediate between B and AB. The latter peak is called a reaction boundary, because the chemical reaction is continuously reequilibrating across it during centrifugal separation of the reactants. The logarithmic velocity per unit field (hereafter referred to simply as velocity) is the constituent sedimentation coefficient of B at the apex; i.e., the average sedimentation coefficient of B in both its forms, free and bound into AB.

Let us now consider the ligand-mediated interaction, $A + B + X \rightleftharpoons ABX$. One might expect, that under certain conditions, the sedimentation pattern of such a system could show three peaks: a slowly sedimenting boundary of A and a more rapidly sedimenting, bimodal reaction boundary. How could this be? The answer resides in the nonlinear coupling between differential transport of the several species and their rapid chemical interconversion. As the complex ABX sediments towards the bottom of the centrifuge cell, the A and B lagging behind react with X to form more ABX which, in turn, outruns A and B. This process eventually depletes the unbound X in the region of the cell centripetal to the sedimenting complex, thereby generating and maintaining against back diffusion a gradient of unbound X across the reaction boundary, whose local macromolecule composition is dictated by mass action. Thus, one can visualize the reaction boundary resolving into two peaks corresponding to different equilibrium compositions, the faster sedimenting peak being rich in ABX and the slower one rich in B. The purpose of the transport calculations reported herein is to ascertain whether the envisioned behavior is theoretically possible and, if so, to consider its implications for ultracentrifugal studies on protein complexes.

3. Results and discussion

Representative sedimentation patterns computed for reaction set 3 are displayed in figs. 1 and 2. It is immediately apparent that, under appropriate conditions, ligand-mediated heterogeneous association-dissociation reactions can give a bimodal reaction boundary as envisioned above. The contrasting sedimentation behavior of associating systems with and without ligand-mediation is illustrated in fig. 1A. Whereas the control pattern a, computed for association without ligand-mediation (reaction set 6), shows a boundary of A and an unimodal reaction boundary sedimenting at a velocity between that AB and ABD, pattern b for ligand mediation (reaction set 3) shows three peaks: a boundary of A and two more-rapidly sedimenting peaks constituting a bimodal reaction boundary. The faster of the two peaks corresponds to an equilibrium mixture rich in ABDX and, thus, sediments between AB and ABDX but closer to the latter; the slower one being rich in AB sediments between B and AB. Comparison of pattern b with the ligand-concentration profile c bears out our proposition that resolution of the bimodal reaction boundary is dependent, through the agency of mass action, upon the generation of a concentration gradient of ligand along the centrifuge cell. Essentially the same results were obtained for the special cases of reaction set 3 in which D is identical with A or B.

These results are for nonstoichiometric proportions of the macroreactants A, B and D; but, as shown in fig. 1B, qualitatively similar patterns were obtained for stoichiometric proportions. Patterns computed for progressively increasing constituent concentration of ligand, the stoichiometric concentrations of macroreactants being held con-

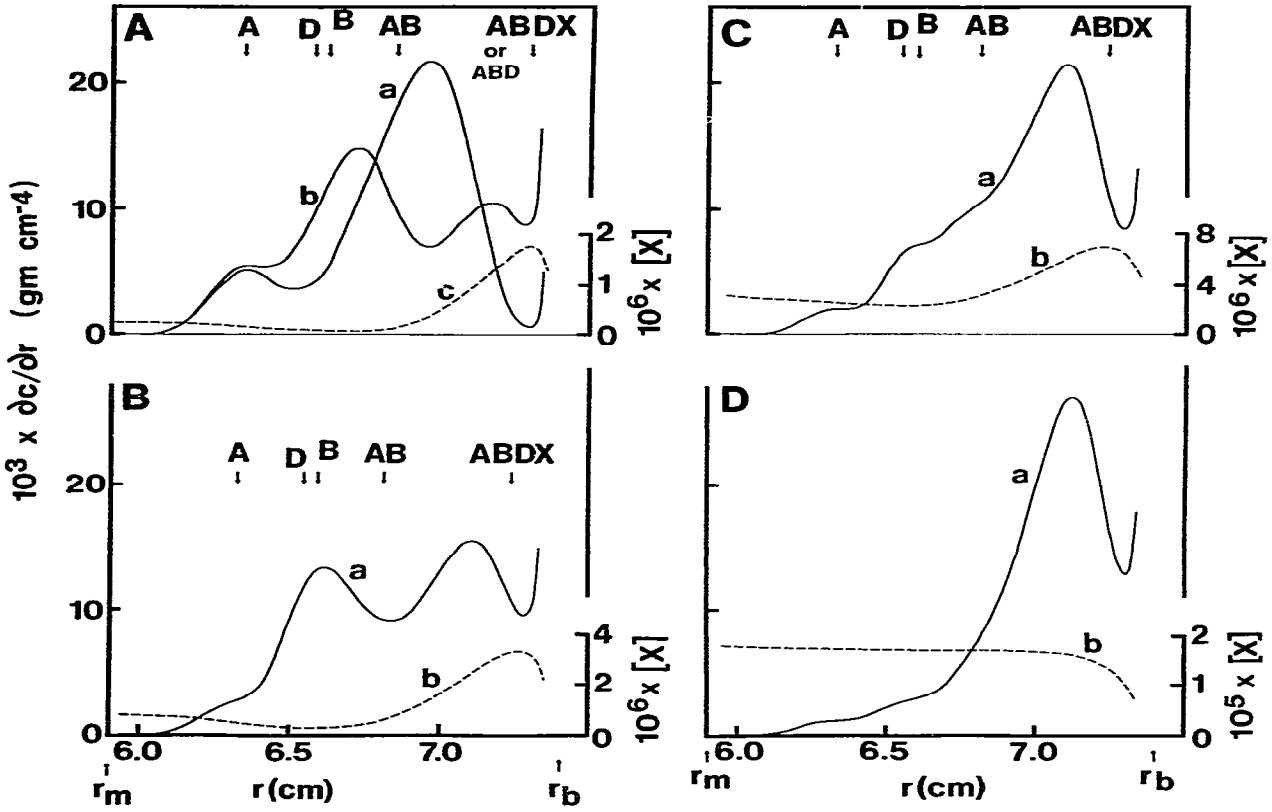

Fig. 1. Theoretical sedimentation patterns for ligand-mediated heterogeneous association-dissociation. (A) Pattern a, control without ligand mediation (reaction set 6); $K_1 = 2\times10^4$ M^{-1}, $K_2 = 4\times10^4$ M^{-1}; $\bar{A} = 0.1$ mM, $\bar{B} = 75$ μM, $\bar{D} = 50$ μM. Pattern b, computed for association mediated in part by a single kind of ligand (reaction set 3); $K_1 = 2\times10^4$ M^{-1}, $K_2 = 2\times10^{10}$ M^{-2}; $\bar{X} = 27$ μM. Curve c, concentration profile of unbound ligand X corresponding to pattern b. (B) Pattern a, computed for reaction set 3; $\bar{A} = \bar{B} = \bar{D} = 75$ μM, $\bar{X} = 40$ μM. Curve b, ligand-concentration profile. (C) Same as B except that $\bar{X} = 51$ μM. (D) $\bar{X} = 75$ μM. $s_A = 3$, $s_B = 4.8$, $s_D = 4.5$, $s_{AB} = 6.2$, $s_{ABD} = s_{ABDX} = 8.8$ S; $D_A = 7\times10^{-7}$, $D_B = 5.6\times10^{-7}$, $D_D = 4.3\times10^{-7}$, $D_{AB} = 4.9\times10^{-7}$, $D_{ABD} = D_{ABDX} = 4.1\times10^{-7}$ cm^2 s^{-1}; $M_A = 4\times10^4$, $M_B = 8\times10^4$, $M_D = 8\times10^4$; $s_X = 0$ S and $D_X = 1\times10^{-5}$ cm^2 s^{-1} in this and following figures. In A, B and D, 50740 rpm and $t = 8.56\times10^3$ s; in C, 60000 rpm and $t = 5.89\times10^3$ s.

stant, are presented in fig. 1B–D. As anticipated, increasing ligand concentration drives association towards completion with concomitant loss of resolution; and it is of interest to note the undulating nature of the centripetal side of the pattern in fig. 1C.

The foregoing calculations assign a fairly wide spread to the values of the sedimentation coefficients of the macroreactants, but in some experimental systems they might be quite similar. In that event, theory predicts that the pattern will show at most two peaks as in patterns a and b of fig. 2A, which were calculated for stoichiometric proportions of macroreactants with low to moderate ligand concentration. The two peaks constitute a bimodal reaction boundary: the fast peak is rich in both AB and ABDX, while the slow one contains chiefly AB and unbound macroreactants. At higher

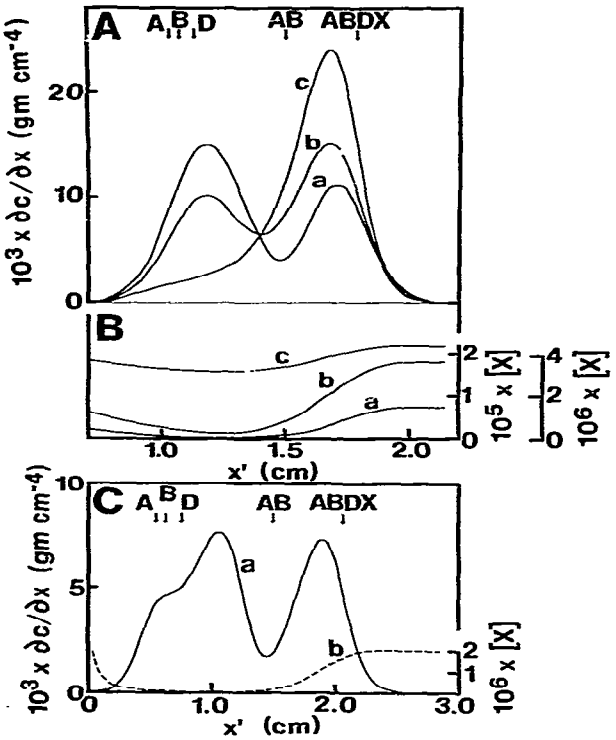

ligand concentration, pattern c shows a rapidly sedimenting unimodal reaction boundary with a centripetal tail composed largely of unbound macroreactants. Thus, it is apparent that, in general, the unbound macroreactants do not express themselves overtly with respect to the gross shape of the pattern. However, this is not so for nonstoichiometric proportions, in which case the bimodal reaction boundary may show a strong centripetal shoulder corresponding to unbound macroreactant (fig. 2C).

Fig. 2. Theoretical sedimentation patterns for heterogeneous association-dissociation mediated in part by a single kind of ligand (reaction set 3). (A) Patterns computed for increasing ligand concentration, stoichiometric concentrations of macroreactants held constant: a, $\bar{X}=27$ μM; b, 40 μM; c, 75 μM. $\bar{A}=\bar{B}=\bar{D}=75$ μM; $K_1=2\times10^4$ M^{-1}, $K_2=2\times10^{10}$ M^{-2}; 60000 rpm; $t=8\times10^3$ s. (B) Ligand concentration profiles: a, b, c and d pair with correspondingly designated patterns in A; a and b, ordinate to far right; c, other ordinate. (C) Pattern a and ligand concentration profile b computed for nonstoichiometric proportions of macroreactants: $\bar{A}=0.1$ mM, $\bar{B}=75$ μM, $\bar{D}=50$ μM; $\bar{X}=27$ μM; 60000 rpm, $t=1.6\times10^4$ s. $s_A=2.5$, $s_B=2.7$, $s_D=3$, $s_{AB}=4.8$, $s_{ABDX}=6.2$ S; $D_A=D_B=D_D=7\times10^{-7}$, $D_{AB}=5.6\times10^{-7}$, $D_{ABDX}=4.9\times10^{-7}$ cm^2 s^{-1}; $M_A=M_B=M_D=4\times10^4$.

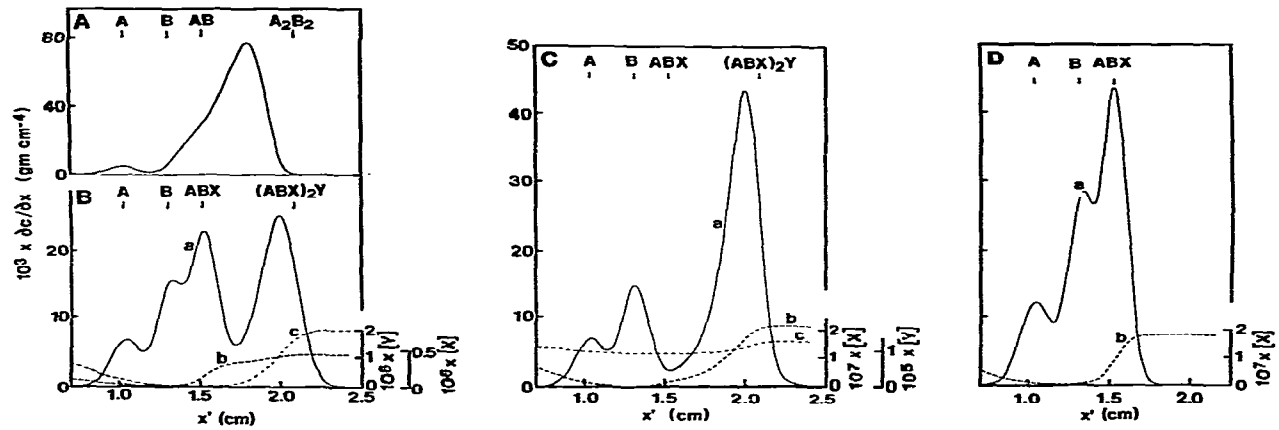

Fig. 3. Theoretical sedimentation patterns for heterogeneous association-dissociation mediated in a stepwise fashion by two different ligands (reaction set 4j. (A) Control without ligand mediation (i.e., analogous to reaction set 4 but without participation of X and Y): $K_1=4\times10^4$ M^{-1}, $K_2=5\times10^3$ M^{-1}; $\bar{A}=\bar{B}=0.25$ mM. (B) Pattern a, ligand X-concentration profile b and ligand Y-concentration profile c computed for reaction set 4: $K_1=8\times10^{10}$ M^{-2}, $K_2=5\times10^9$ M^{-2}; $\bar{A}=\bar{B}=0.138$ mM; $\bar{X}=0.1005$ mM, $\bar{Y}=27$ μM. (C) Same as B except that $\bar{X}=50.25$ μM. (D) $\bar{X}=10$ nM. $s_A=3$, $s_B=4.8$, $s_{ABX}=6.2$, $s_{(ABX)_2Y}=9.8$ S; $D_A=7\times10^{-7}$, $D_B=5.6\times10^{-7}$, $D_{ABX}=4.9\times10^{-7}$, $D_{(ABX)_2Y}=3.9\times10^{-7}$ cm^2 s^{-1}; $M_A=4\times10^4$, $M_B=8\times10^4$, $s_Y=0$ S and $D_Y=1\times10^{-5}$ cm^2 s^{-1} in this and the following figure; 60000 rpm and $t=6\times10^3$ s.

So far we have considered heterogeneous association mediated in part by a single kind of ligand. Intuitively, one would expect that the involvement of two different ligands could give rise to an even more complex behavior. This is borne out by the sedimentation patterns computed for reaction set 4 and displayed in fig. 3. Here all calculations were made for stoichiometric proportions of the macroreactants A and B. The control pattern for nonmediated association (fig. 3A) shows a small boundary of A and a unimodal reaction boundary with a peak velocity between AB and A_2B_2 and a slight shoulder between B and AB. In contrast, pattern a presented in fig. 3B for mediation by two ligands exhibits four peaks: a boundary of A and a trimodal reaction boundary. The slowest sedimenting peak of the reaction boundary sediments slightly faster than B because it corresponds to an equilibrium mixture containing some ABX. The next faster peak sediments at the velocity of ABX, although this is fortuitous, since the equilibrium composition includes a small amount of $(ABX)_2Y$ as well as A and B, the concentration of all species changing across the peak. The fastest peak sediments slower than $(ABX)_2Y$, because the concentration of ABX also changes somewhat across the peak. In other words, the velocity of each peak in the reaction boundary is the average velocity of the equilibrium mixture at its apex, whose composition is determined by the local concentration of ligands. Conversely, resolution is dependent upon generation and maintenance of concentration gradients of both ligands, and comparison of the ligand concentration profiles b and c reveals their coupling in the region of the fastest peak. This coupling is a consequence of mass action as applied to the two consecutive reactions comprising reaction set 4.

There are two limiting cases of reaction set 4, which give sedimentation patterns showing only three peaks. The first case is for high concentration of ligand Y (fig. 3C). The two slowest peaks in pattern a are boundaries of pure A and essentially pure B, which are virtually uncoupled in this region of the centrifuge cell due to depletion of ligand X (profile b). The third peak is a unimodal reaction boundary rich in $(ABX)_2Y$. In the other limit, the concentration of ligand Y is vanishingly small so that reaction set 4 collapses to A + B + X $\rightleftharpoons$ ABX. The pattern in fig. 3D shows the boundary of A and the bimodal reaction boundary envisioned early on for this particular interaction.

Let us now turn our attention to self-association mediated by two different ligands acting in a stepwise fashion, reaction set 5. The computed sedimentation patterns are presented in fig. 4. Whereas the control pattern for self-association without ligand mediation shows a unimodal reaction boundary (pattern a in fig. 4B), the pattern for ligand mediation exhibits a trimodal reaction boundary (pattern a in fig. 4A and pattern b in fig. 4B). * The slowest peak in the reaction boundary sediments slightly faster than monomer; the central peak, slower than dimer; and the fastest peak, slower than tetramer. As for the mechanism of resolution, the ligand-concentration profiles in fig. 4A or B are similar in shape to those found for heterogeneous association (fig. 3B) and speak for themselves.

Increasing the constituent concentration of ligand Y, all other parameters being held constant, drives self-association towards tetramer. As a consequence, the central peak of the trimodal reaction boundary, a peak rich in dimer, disappears (fig. 4C). A bimodal reaction boundary is also occasioned by decreasing the strength of the interactions (fig. 4D) **. Finally, in the limit of vanishingly low concentration of ligand Y, reaction set 5 collapses to ligand-mediated dimerization (reaction 5a), which also shows a bimodal reaction boundary; but, in contrast to the patterns in fig. 4C and D, the leading peak sediments slower than dimer with its companion sedimenting faster than monomer. This result agrees with our previous calculations [1–4].

The several results described above have important implications for both fundamental studies on subunit proteins and protein assemblies, and conventional ultracentrifugal analysis. With respect to fundamental studies, theory predicts that

* An exploratory calculation showed that reaction set 5 can also give a trimodal reaction zone.

** As expected [4], a similar bimodal pattern was obtained by specifying [Y]≡[X] so as to form the tetramer M_4X_2.

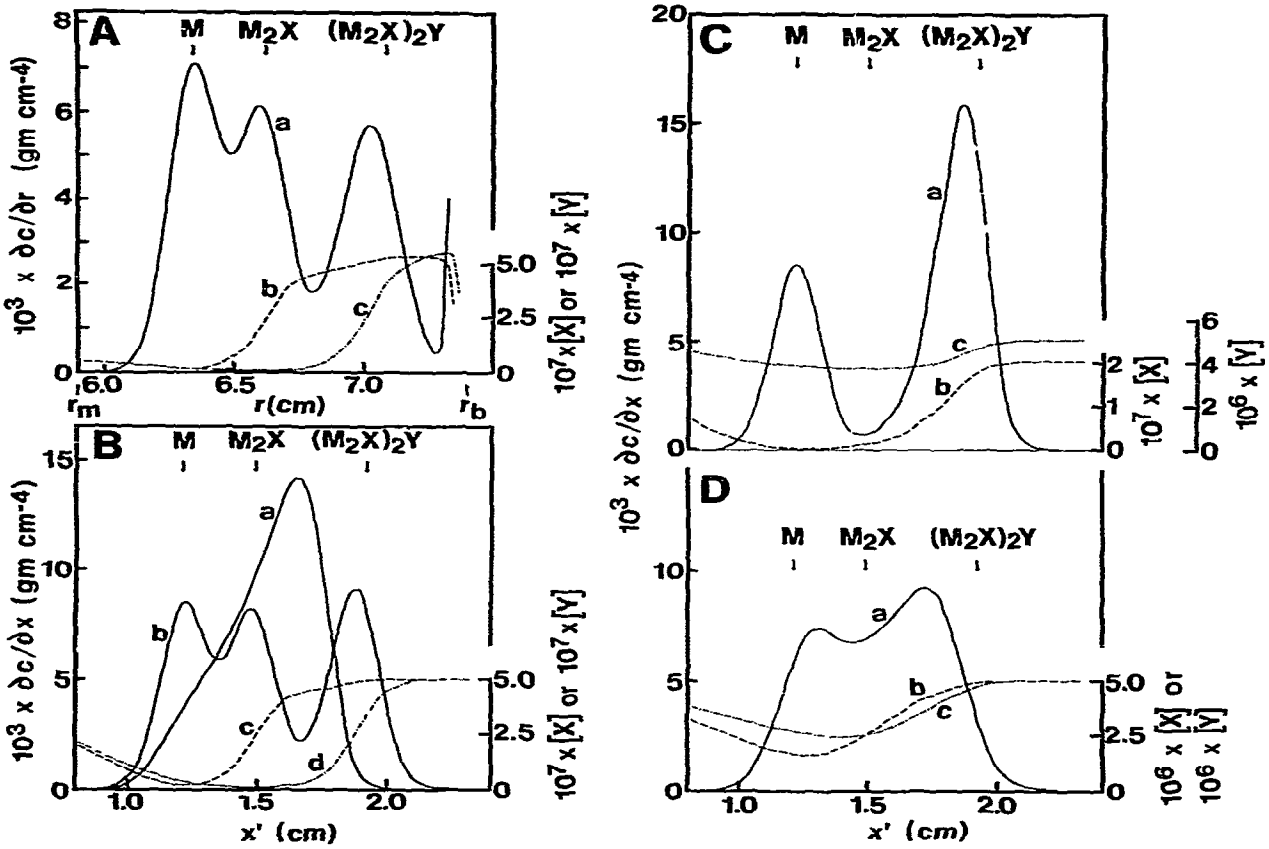

Fig. 4. Theoretical sedimentation patterns for self-association mediated in a stepwise fashion by two different ligand (reaction set 5). (A) Pattern a, ligand X-concentration profile b and ligand Y-concentration profile c calculated for a sector-shaped cell: $K_1 = 2\times10^{10}$ M^{-2}, $K_2 = 4\times10^{10}$ M^{-2}, $\bar{M} = 0.15$ mM, $\bar{X} = 50.5$ μM, $\bar{Y} = 13$ μM. (B) Pattern a, control without ligand mediation (i.e., analogous to reaction set 5 but without participation of X and Y): $K_1 = 1\times10^4$ M^{-1}, $K_2 = 2\times10^4$ M^{-1}; $M = 0.15$ mM. Pattern b, ligand X-concentration profile c and ligand Y-concentration profile d are for the same system as in A, but calculated to the rectilinear-constant field approximation. (C) Same as the ligand-mediated system shown in B except that $\bar{Y} = 25.25$ μM. (D) Pattern a, ligand X-concentration profile b and ligand Y-concentration profile c calculated for a 10-fold weaker interaction than in A and B: $K_1 = 2\times10^9$ M^{-2} and $K_2 = 4\times10^9$ M^{-2}; $\bar{M} = 0.15$ mM, $\bar{X} = 55$ μM; $\bar{Y} = 17.5$ μM. $s_M = 3$, $s_{M_2X} = 4.8$, $s_{(M_2X)_2Y} = 7.6$ S; $D_M = 7\times10^{-7}$ $D_{M_2X} = 5.6\times10^{-7}$, $D_{(M_2X)_2Y} = 4.4\times10^{-7}$ cm^2 s^{-1}; $M_M = 4\times10^4$; 60000 rpm; $t = 6.12\times10^3$ s in A and 6×10^3 s in B–D.

ligand-mediated heterogeneous association-dissociation reactions and self-association can give multimodal reaction boundaries. Careful note should be taken that the peaks comprising a reaction boundary correspond to different equilibrium compositions and not to individual protein species. Accordingly, in general, their sedimentation velocities are not characteristic molecular parameters of products or reactants, nor can their areas be used to calculate association constants. On the other hand, significant mechanistic insights can be obtained by varying the proportions of protein reactants and the constituent concentration of ligand(s) which promotes their association. But,

since the generation of bimodal and multimodal reaction boundaries is not unique for any one reaction mechanism, it is imperative that several independent physicochemical methods be brought to bear in order to establish the exact nature of the interaction. In this regard, factors other than ligand mediation can give rise to sedimentation patterns showing multiple peaks. These include slow reaction rates [10,23] and microheterogeneity of one or more of the reactants with respect to association constant [23,24].

As for conventional ultracentrifugal analysis, many of the patterns displayed in figs. 1–4 for ligand-mediated associations bear a strong resemblance to patterns shown by mixtures of noninteracting proteins. This demonstrates yet again that proof for inherent heterogeneity ultimately depends upon isolation of the various components [1,10,25]. In a related vein, the results for ligand-mediated self-association could conceivably have import for active enzyme sedimentation [26] in solutions containing inhibitors, cofactors or allosteric affectors, which might promote association of the enzyme as in the case of carbamoyl-phosphate synthetase from *E. coli* [27].

Acknowledgements

This work was supported in part by Research Grant R01 GM28793-30 from the National Institute of General Medical Sciences, National Institutes of Health, U.S. Public Health Service.

References

1 J.R. Cann and W.B. Goad, Science 170 (1970) 441.
2 J.R. Cann, Interacting macromolecules. The theory and practice of their electrophoresis, ultracentrifugation, and chromatography (Academic Press, New York, 1970) p. 196.
3 J.R. Cann and W.B. Goad, Arch. Biochem. Biophys. 153 (1972) 603.
4 J.R. Cann, Biophys. Chem. 1 (1973) 1.
5 G.A. Gilbert, Disc. Faraday Soc. 20 (1955) 68.
6 G.A. Gilbert, Proc. R. Soc. (Lond.) Ser. A 250 (1959) 377.
7 E.O. Field and J.R.P. O'Brien, Biochem. J. 60 (1955) 656.
8 E.O. Field and A.G. Ogsten, Biochem. J. 60 (1955) 661.
9 J.L. Bethune and G. Kegeles, J. Phys. Chem. 65 (1961) 433.
10 J.R. Cann and G. Kegeles, Biochemistry 13 (1974) 1868.
11 G.C. Na and S.N. Timasheff, Biochemistry 19 (1980) 1347 and 1355.
12 T.E. Palmer and K.E. Neet, Arch. Biochem. Biophys. 205 (1980) 412.
13 N.C. Brown, A. Larsson and P. Reichard, J. Biol. Chem. 242 (1976) 4272.
14 R.C. Valentine, B.M. Shapiro and E.R. Stadtman, Biochemistry 7 (1968) 2143.
15 S.S. Margossian and C. Cohen, J. Mol. Biol. 81 (1973) 409.
16 J. Gergely, Basic Res. Cardiol. 75 (1980) 18.
17 S.S. Margossian and S. Lowey, Biochemistry 17 (1978) 5431.
18 L.E. Green, Biochemistry 20 (1981) 2120.
19 L. Castellani, E.P. Morris and E.J. O'Brien, Biochem. Biophys. Res. Commun. 96 (1980) 558.
20 D.C. LaPorte, B.M. Wierman and D.R. Storm, Biochemistry 19 (1980) 3814.
21 W.B. Goad, in: Interacting macromolecules. The theory and practice of their electrophoresis, ultracentrifugation, and chromatography, ed. J.R. Cann (Academic Press, New York, 1970) p. 207.
22 J.R. Cann and D.I. Stimpson, Biophys. Chem. 7 (1977) 103.
23 J.R. Cann, Mol. Immunol. 19 (1982) 505.
24 J.B. Chaires and G. Kegeles, Biophys. Chem. 7 (1977) 173.
25 J.R. Cann, Interacting macromolecules. The theory and practice of their electrophoresis, ultracentrifugation, and chromatography (Academic Press, New York, 1970) p. 224.
26 D.J. Winzor, in: Protein-protein interactions, eds. C. Frieden and L.W. Nichol (John Wiley and Sons, New York, 1981) p. 154.
27 P.M. Anderson and S.V. Marvin, Biochemistry 9 (1970) 171.